Engineered Science
DOI: https://dx.doi.org/10.30919/es1863

Characterization of Heat Transfer Enhancement and Flow Topology in a Three-Start Spirally Corrugated Tube

Yuexiang Du,[1] Arnut Phila,[2] Pitak Promthaisong,[3] Varesa Chuwattanakul[4,*] and Smith Eiamsa-ard[2]

Abstract

The article provides a numerical analysis of the heat transfer characteristics and laminar periodic flow in a three-dimensional 3-start spirally corrugated tube. The working fluid is air, with a flow rate in terms of Reynolds numbers (*Re*) that ranges from 200 to 2,000. The investigation is conducted at six different pitch ratios (*PR* = 0.75, 1.0, 1.25, 1.5, 2.0, and 2.5) and five different depth ratios (*DR* = 0.02, 0.04, 0.06, 0.08, and 0.10). The results indicated that the spiral flow along the tube length was generated by the 3-start spirally corrugated tube. The swirl flow is divided into two components: the primary swirl flow, which is visible at the core, and the secondary swirl flow, which is visible at the near wall. These components contribute to the enhancement of fluid mixing, boundary layer disruption, and heat transfer on the tube wall. The Nusselt number (*Nu*) and friction factor (*f*) were increased as a result of the decrease in *PR* and the increase in *Re* and *DR*. The range of the Nu/Nu_0, f/f_0, and thermal performance factor (*TPF*) in a range analysis is 1.02 - 15.90, 0.97 - 5.52, and 0.73 - 2.33, respectively. At *Re* = 2,000, the corrugated tube with *DR* = 0.10 exhibited the greatest TPF of 2.33. Additionally, the results indicate that the 3-start spirally corrugated tube significantly improves heat transfer compared to the corresponding straight tube. The findings suggest that the structural characteristics of the flow path within the tube can be changed by a suitable *PR* and *DR* to optimize the overall heat transfer rate and thermal performance factor.

Keywords: Heat transfer; Laminar flow; Three-start corrugated tube; Thermal performance; Swirl flow.
Received: 06 September 2025; Revised: 28 October 2025; Accepted: 06 November 2025
Article type: Research article.

1. Introduction

In both industrial production and daily life, heat transfer is critically important. Heat exchangers are extensively employed in industrial sectors including aerospace, power plants, refrigeration, and automobiles[1,2] as the primary component of heat exchange. A significant device for the implementation of the heat transfer process is the heat exchanger. The adoption of reasonable and effective methods to enhance the heat transfer efficiency of heat exchangers in order to meet the more compact and efficient requirements has been widely used due to its robust structure, extensive applications, easy processing, and low cost, which has been necessary with the development of technology. The influence and constraints of specific working conditions render the utilization of methods that can enhance heat transfer efficiency without the need for external additional energy more appealing to researchers.[3-5] Of these, the spirally corrugated tube is a variety of enhanced heat transfer tube that exhibits exceptional performance. The surface morphology of heat transfer tubes can be altered through the use of corrugations and dimples.[6-9] Corrugations have been effectively applied to the surface of heat transfer tubes due to their simplicity of processing. However, a significant quantity of research is still being conducted to investigate the mechanism by which corrugations improve THCP.

Several researchers have developed modifications to the geometry or shape of corrugated tubes to enhance the rate of heat transfer and thermal performance in a heat exchanger. These modifications can be seen in Fig. 1, which depicts the various tube shapes. Tang *et al.*[10] numerically studied the gas-liquid tubular heat exchanger's hydrodynamic and thermal performance with directionally varying twisted oval tubes. They examined how the twisting angle, twisting direction, and the flow rate influenced the overall performance. The directional varying twisted oval tubes augmented the fluid mixing and increased the heat transfer. Compared to the circular tubular, directionally varying twisted oval tubes would increase the Nusselt numbers and overall performance factor by 5.8%-10.2% and 7.4%-10.7%, respectively, and decrease the friction factor by 5.0%-7.8% within the velocity

[1]*School of Mechanical and Electrical Engineering, Quanzhou University of Information Engineering, Quanzhou, Fujian, 362000, China*
[2]*School of Engineering and Industrial Technology, Mahanakorn University of Technology, Bangkok, 10530, Thailand*

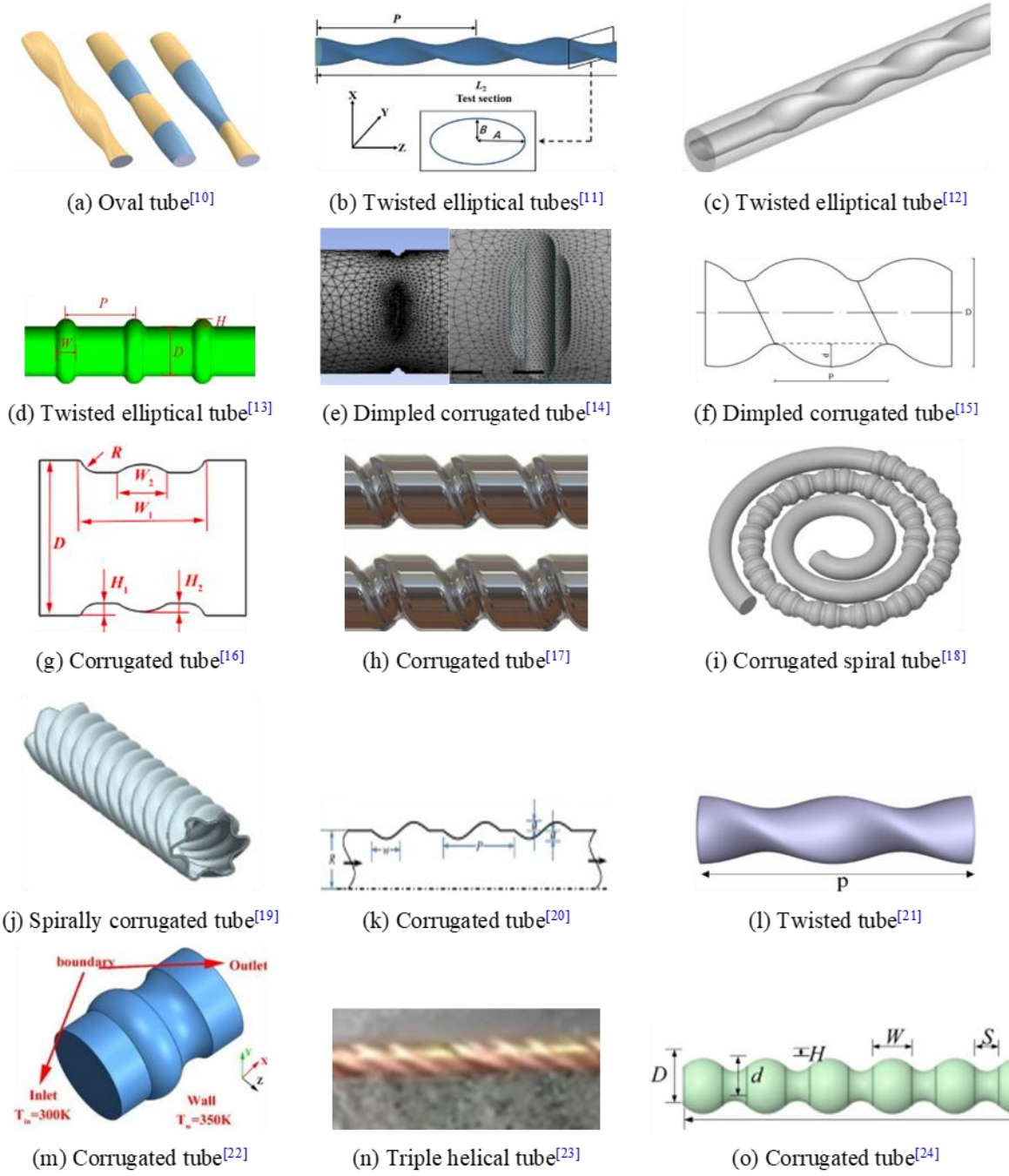

(a) Oval tube[10] (b) Twisted elliptical tubes[11] (c) Twisted elliptical tube[12]

(d) Twisted elliptical tube[13] (e) Dimpled corrugated tube[14] (f) Dimpled corrugated tube[15]

(g) Corrugated tube[16] (h) Corrugated tube[17] (i) Corrugated spiral tube[18]

(j) Spirally corrugated tube[19] (k) Corrugated tube[20] (l) Twisted tube[21]

(m) Corrugated tube[22] (n) Triple helical tube[23] (o) Corrugated tube[24]

Fig. 1: Previous works of modified corrugated tubes.

of 5-9 m/s. Li *et al.*[11] numerically studied the heat flow characteristics of the twisted elliptical tubes. Reynolds numbers ranged from 710 to 4,790. Their study reveals that heat transfer, friction factor, and total entropy generation increased with the rise of the Reynolds number and aspect ratio while decreasing with the rise of twist ratio and aspect ratio. The Nusselt number and pressure drop obtained the highest value when the aspect ratio was 2.16 and the twisted ratio was 11.9. The lowest total entropy generation was obtained when the aspect ratio was 1.34 and the twisted ratio was 26.33. Azizi *et al.*[12] carried out a numerical study to investigate how twisting elliptical tubes influenced the thermo-fluid characteristics in a dual-pipe heat exchanger. The parameters of aspect ratio, even and uneven twisting pitches of the twisting elliptical tube were taken into comparison, as well as the flow arrangement. Their result demonstrates that the increasing aspect ratio and decreasing even twisting pitch,

[3]*Heat Pipe and Thermal Tool Design Research Unit (HTDR), Faculty of Engineering, Mahasarakham University, Maha Sarakham, 44150, Thailand*

[4]*School of Engineering, King Mongkut's Institute of Technology Ladkrabang, Bangkok, 10520, Thailand*

**Email:* varesa.ch@kmitl.ac.th (Varesa Chuwattanakul)

would enhance the heat transfer and the pressure drop. The counter-flow provided better heat transfer by 2-4% without increasing pressure drop compared to the parallel flow. The uneven twisting pitches, which had a pitch of 100 - 200 - 400mm arranged in parallel flow, obtained a high-performance assessment criterion. The counter-flow arranged twisting elliptical tube with a twisting pitch of 100 mm, would give the highest performance assessment criterion of 1.166. Cai *et al*.[13] investigated how the height-to-diameter ratio of the corrugation (*H/D*), the pitch-to-diameter ratio (*P/D*), and the width-to-diameter ratio (*W/D*) affect the thermofluid characteristics of ice slurry in a tube with outward transverse corrugations (OTCT). The outcome illustrated that a higher *H/D* and lower *P/D* and *W/D* would induce better vortical structure in turbulent flow and better ice particle distribution. A similar trend was also observed in the variations of the average Nusselt number and the friction factor. The highest overall thermal performance was achieved at a Reynolds number of 9540, a *W/D* of and an ice volume fraction at the inlet of 10%. The heat transfer and friction factor of nanofluids in tubes featuring dual spherical dimples were studied by Ahmad *et al*.[14] The single nanofluids (CuO/water, *etc*.) and composite nanofluids (Al_2O_3-CuO/water, *etc*.) at various nanoparticle concentrations of 1%-3% were studied. The Nusselt number ranged from 10,000 to 30,000. The dual spherical dimples disrupted laminar flow, which would augment the heat transfer. Their result revealed that dual-dimpled tubes with different nanoparticles augmented the heat transfer coefficient by 20–25% compared to the plain tubes. The Nusselt number rose by the dual spherical dimple structures when the nanoparticle concentrations were higher. All studied corrugated tubes have a performance evaluation criterion over unity. The nanoparticle concentration of 3% Al_2O_3-CuO/water hybrid nanofluid performed best, obtaining a 20.62% thermal performance index.

Moya-Rico *et al*.[15] carried out a numerical study on the thermal hydraulics performance in the dual tube heat exchanger (DTHX) 21 cases, including plain tubes and inner and outer corrugated tubes, were examined. A sugar–water mixture with a Brix concentration of 60° was employed as the working fluid. The results illustrated that the velocity and the corrugation parameters would affect the heat transfer. Outer corrugations with small groove dimensions enhanced heat transfer, with a 5% improvement in average efficiency and performance over the smooth shell. And the deeper grooves had no effect. For the inner tube, the deepest configurations, which had a groove depth of 1.1 mm (CO_{11}) and 1.2 mm (CO_{12}), performed best, with CO_{12} achieving a 19% efficiency gain and CO_{11} a 9% improvement compared to the smooth tube. Liao *et al*.[16] numerically studied how the compound corrugation affected the thermal performance of corrugated tubes. The Reynolds number range was from 5,000 to 30,000. The width (W_2) and depth (H_2) of the compound corrugation were examined. The outcome reveals that the compound corrugation performed better in turbulent kinetic energy and Nusselt number than the simple corrugation by 22% and 10.1%, respectively, and the heat transfer increased with the rising of W_2 and H_2. The highest Nusselt number ratio (2.15) was observed with a width to diameter of 0.3 and depth to diameter of 0.05. Kirkar *et al*.[17] examined how the corrugating pitches of 6 mm, mm,12 mm, and 18 mm and depths of 0.6 mm, 0.8 mm, and 1.0 mm influenced the heat transfer, friction factor, and the overall thermal performance numerically. The Reynolds number ranged from 480 to 6,100, and water was used as the testing fluid. They found that the corrugation induced better heat transfer than a plain tube did in the laminar flow. The best overall thermal performance was 2.48. A numerical study was conducted to simulate the heat transfer and fluid flow performance in corrugated spiral tubes with various corrugation patterns by Elboughdiri *et al*.[18] The corrugation patterns, including inner, outer and the inner-outer combined configuration, were taken into study to compare with a smooth tube. The results indicated that the inner corrugation significantly enhanced the heat transfer, which led to a 53% increase. The Nusselt number rose with the increasing of corrugation height, and so did the friction factor, which led to a reduction of the thermal performance factor. The highest thermal performance factor value was observed at a corrugation width ratio of 0.1. The increase in the corrugation pitch improved the heat transfer. And the inner corrugation yielded the highest value. But the outer corrugation provided the best thermal performance. Yang *et al*.[19] numerically analysed how the start number, groove depth and groove pitch affected the heat transfer in a corrugated tube. It was observed that secondary flow caused by the corrugation near the wall enhanced the heat transfer. The average heat transfer coefficient was enhanced by 36.3% when the depth increased from 1mm to 3 mm. Meanwhile, increasing the corrugation pitch from 9 mm to 13 mm would lead to a 4.8% reduction in the average heat transfer coefficient. For the four-start corrugated tube, the optimal parameter combination of corrugation depth of 3 mm and pitch of 9 mm resulted in heat transfer enhancements of 15% and 4.9% at Reynolds numbers Re = 30,000 and 60,000, respectively.

Kumar *et al*.[20] evaluated the entropy production and thermohydraulic performance of corrugation tubes with various corrugation starting profiles. The findings demonstrated that different initial corrugation types would result in different entropy production and thermohydraulic performance. In all flow velocity conditions, the inward-outward arc corrugations led to the highest Nusselt number and better heat transfer performance but a higher friction factor. Under the condition of a high Reynolds number, the outward arc-inward arc configuration resulted in the lowest entropy production of 0.398 W/K. The total entropy production was below 1.0 for all studied cases. Ghazanfari *et al*.[21] numerically compared the twisting tube's thermohydraulic performance in a helical coil heat exchanger with a plain tube. They investigated the influence of the flow velocity, pitches and twisted tube configurations on the heat transfer and

pressure drop. It was observed that a higher Reynolds number would result in a pressure drop reduction of 25% and a heat transfer coefficient increase of 35%. A pitch of 5.5mm proved to be the optimal option for better balance between the heat transfer enhancement and pumping cost. At lower Reynolds numbers, twisted tubes showed significant performance advantages, with Performance Evaluation Criterion (PEC) values 20–33% higher than those of smooth circular tubes. But this advantage diminishes at higher Reynolds numbers, with PEC augmentation lower than 10%. When using a counter-flow twisted tube configuration, the Nusselt number increases by approximately 13%, the friction factor rises by 11%, and the overall PEC is enhanced by 10%.

Liao, Jing and Lian[22] numerically analyzed the effects of simple and compound corrugations on the thermal and hydraulic performance. Their findings demonstrated that the compound corrugations enhanced thermal and hydraulic performance by enhancing the fluid's impact on the tube wall, breaking the boundary layer and enlarging the secondary flow area. At a Reynolds number of 20,000, the compound corrugated tube achieved a performance evaluation criterion (PEC) value 1.315 times that of the simple corrugated tube. Abdelmagied *et al*.[23] numerically and experimentally studied the influence of a twisted tube in triple-helical-tube (THTITT) on the thermal and exergy performance. Compared to the earlier double helical twisted tube-in-tube (DHTITT), THTITT induced an additional fluid stream and a twisted inner tube to increase interfacial surface area and temperature gradients among the three fluids. The effects of twist pitch ratio, hydraulic diameter, coil torsion angle, inclination angle, and Dean number were established to investigate. Results showed that THTITT enhanced the Nusselt number by 61.8% over DHTITT, with minimal increase in friction factor. Han *et al*.[24] carried out a numerically simulation. They analyzed the fouling behavior in corrugated tubes with various corrugation parameters. They investigated the influences of corrugation height, width, and pitch on local fouling thermal resistance. The results indicated that corrugated tubes had significantly better antifouling performance than smooth tubes, with an average local fouling resistance 27% lower. The fouling resistance showed a periodic distribution along the tube length. with max. located at the upstream of the converging section obtained the highest value, and the lowest value was observed in the middle. Increasing corrugation height reduced local fouling resistance, whereas greater width and pitch led to higher resistance. Overall, corrugation height was found to be the most influential parameter in fouling suppression. Chithra *et al*.[25] investigated twisted square ducts combined with a twisted tape to evaluate thermal performance in the laminar flow region. They found that the test ducts generated swirl flow both in the spanwise plane and as a continuous swirling motion along the duct. This swirl flow significantly enhanced flow mixing near the duct wall, leading to an improved heat transfer rate compared to smooth square ducts. The maximum TPF was found to be 1.44 at Re = 1500. Guo and Wang[8] investigated twisted elliptical tubes with various cross-sectional areas to enhance thermal performance in laminar forced convective heat transfer. They reported that the twisted elliptical tubes induced secondary flows and provided higher convective heat transfer than smooth, straight elliptical tubes. The maximum *TPF* was found to be 1.6 at Re = 1,500.

Previous studies showed that the corrugated tube heat transfer enhancement can effectively disrupt the thermal boundary layer through the periodic concave-convex structure of the corrugated tube, promoting fluid mixing. Moreover, compared with linear, uniform circular tubes, the corrugated tube increased the surface area, thereby expanding the heat transfer area. Compared with the inserted turbulators, the corrugated tube has a relatively milder pressure drop under the same heat transfer enhancement effect, and had a higher heat transfer performance factor, which means lower pumping consumption and lower energy loss. However, this technology still needs to be considered in terms of heat transfer trade-offs, and it is sensitive to geometric parameters. The heat transfer performance depends largely on the shape of the corrugation and the geometric parameters of the corrugation. In addition, most investigations focus on the turbulent flow region, while the effect on heat transfer performance in the laminar flow region has rarely been reported. Moreover, the engineering applications where the corrugated tube heat exchangers were used in laminar flow include: the food and beverage industry (heat exchangers for pasteurization or sterilization) and the pharmaceutical and biotechnology processes (the corrugated tube help increase heat transfer performance while maintaining gentle flow conditions to avoid damaging the product). Consequently, the primary objective of this article is to investigate the impact of a newly designed three-dimensional 3-start spirally corrugated tube with a variety of pitch ratios (PR = 0.75, 1.0, 1.25, 1.5, 2.0, and 2.5) and five distinct depth ratios (DR = 0.02, 0.04, 0.06, 0.08, and 0.10) in the laminar flow region using numerical simulation technique. The mechanism of flow structure, pressure loss, and heat transmission can be more effectively comprehended by twisting the corrugated tube in this study. The working fluid in the current study is air, with a flow rate in units of Reynolds numbers that ranges from 200 to 2,000. A comparison is made between the numerical results and the linear, uniform circular tube.

2. Mathematical foundations

The numerical model for fluid flow and heat transfer in the tube is developed under the following assumptions: fluid flow and heat transfer are in three-dimensional steady conditions, the flow is laminar and incompressible, fluid properties are constant, and body force, viscous dissipation as well as radiation heat transfer are negligible. Based on the above assumptions, the tube flow is governed by the continuity, the Navier-Stokes and the energy equations. In the Cartesian tensor system these equations can be written as follows Eqs. (1-4):

Continuity equation:

$$\frac{\partial}{\partial x_i}(\rho u_i) = 0 \tag{1}$$

Momentum equation:

$$\frac{\partial(\rho u_i u_j)}{\partial x_j} = \frac{\partial}{\partial x_j}\left[\mu\left(\frac{\partial u_i}{\partial x_j} + \frac{\partial u_j}{\partial x_i}\right)\right] - \frac{\partial p}{\partial x_i} \tag{2}$$

Energy equation:

$$\frac{\partial}{\partial x_j}(\rho u_j T) = \frac{\partial}{\partial x_j}\left(\Gamma \frac{\partial T}{\partial x_j}\right) \tag{3}$$

where Γ is the thermal diffusivity and is given by $\Gamma = \mu / Pr$

All the governing equations can be re-organized and expressed in a standard form that includes the convection, diffusion, and source terms for three-dimension flows as follows

$$\frac{\partial}{\partial x}(\rho u\varphi) + \frac{\partial}{\partial y}(\rho v\varphi) + \frac{\partial}{\partial z}(\rho w\varphi) - \frac{\partial}{\partial x}\left(\Gamma_{\varphi x}\frac{\partial \varphi}{\partial x}\right) - \frac{\partial}{\partial y}\left(\Gamma_{\varphi y}\frac{\partial \varphi}{\partial y}\right) - \frac{\partial}{\partial z}\left(\Gamma_{\varphi z}\frac{\partial \varphi}{\partial z}\right) = S_\varphi \tag{4}$$

In the numerical simulation of heat transfer and fluid dynamics, the system of algebraic equations derived from discretized governing equations can be solved for each variable through an iterative relaxation process, with coefficients updated via the Tri-Diagonal Matrix Algorithm (TDMA) or other efficient linear solvers (such as the Gauss-Seidel iteration). The main challenge in solving the velocity field is the implicit coupling of the pressure field: the gradient of pressure term in the Navier-Stokes equations inspires the velocity field, which means that the solution of momentum equations depends on the unknown distribution of pressure. To solve this significant coupling problem, this study uses the Patankar and Spalding[26]-proposed SIMPLE (Semi-Implicit Method for Pressure-Linked Equations) approach. The approach accomplishes the iterative decoupling of the pressure and velocity fields by building a pressure correction equation and incorporating continuity restrictions. A coupled technique within the pressure-based solver is used to update the pressure field and velocity components simultaneously for the three-dimensional numerical model built on the ANSYS FLUENT platform. To ensure the solution accuracy of thermophysical processes, the energy conservation equation is assigned a convergence criterion of 10^{-6} more stringent than the 10^{-5} criterion for other transport equations (momentum, continuity, and turbulence). This hierarchical convergence strategy effectively suppresses the accumulation of energy non-conservation errors while maintaining computational efficiency, proving particularly suitable for simulations sensitive to temperature gradients, such as phase-change heat transfer and conjugate heat conduction.

3. Numerical Method

3.1 Geometric shape simulation of 3-start spirally corrugated tube

The 3-start spirally corrugated tube is formed by modifying the shape of a straight tube as seen in Fig. 2. The tube's diameter and length are defined as *D* and *L*. This study aims to investigate the heat transfer enhancement of the 3-start spirally corrugated tube with varying corrugation dimensions by comparing the results with those of the smooth tube. Fig. 2 depicts the computational domain and structural schematic of the model. Parameters for the 3-start spirally corrugated tube include the pitch ratio and five distinct depth ratios. Specifically, the pitch-to-diameter ratio (*p/D*, or *PR*) is 0.75, 1.0, 1.25, 1.5, 2.0, and 2.5, while the depth-to-diameter ratio (*e/D*, or *DR*) is 0.02, 0.04, 0.06, 0.08, and 0.10. The pitch (*p*) is defined as the helical length over a 360° rotation. The depth of groove corresponds to the depth (*e*) of the helical elliptical tube. The study investigates the 3-start spirally corrugated tubes with the aforementioned parameters over the Reynolds number (*Re*) range of 200–2,000. Details of the geometric configuration are provided in Table 1.

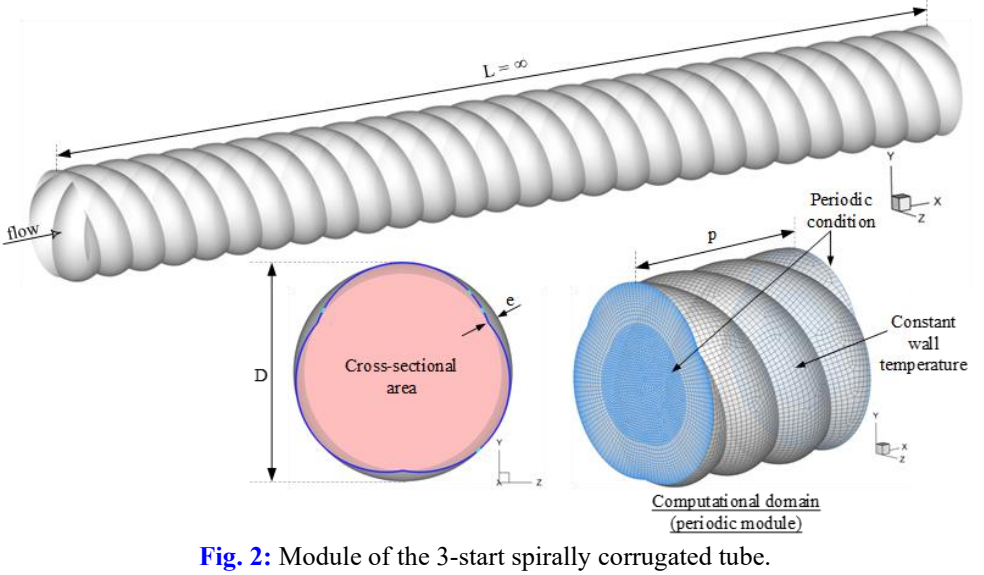

Fig. 2: Module of the 3-start spirally corrugated tube.

Table 1: Geometric details of the 3-start spirally corrugated tube.

Type of tube	*PR*	*DR*
3-start spirally corrugated tube	0.6, 0.8, 1.0, 1.5, 2.0, 2.5, 3.0, 3.5,4.0	0.03, 0.04, 0.05, 0.06, 0.07, 0.10, 0.15,0.20

3.2 Boundary conditions

This study investigates the airflow characteristics in a 3-start spirally corrugated tube which is constructed from copper. The numerical setup adopts periodic boundary conditions at the inlet and outlet of the flow domain. A constant mass flow rate of air at 300 K is assumed in the flow direction rather than a constant pressure drop due to periodic flow conditions. The inlet and outlet profiles for the velocities are assumed to be identical. The physical properties of the air are evaluated at average bulk temperature. Impermeable boundary and no-slip wall conditions have been implemented over the tube wall as well as the baffle. It should be noted that the inlet and outlet dimensionless temperatures are set to be the same. The computational results are shown in the topologies of flow and heat transfer.

3.3 Parameters

In this research, the Reynolds number (*Re*), friction facto (*f*), local and average Nusselt numbers (Nu_x and *Nu*), and thermal performance factor (*TPF*) are selected as critical parameters. The mathematical expressions are given in Eq. (5) to (12).[26,27], sequentially:

$$Re = \frac{\rho \bar{u} D_h}{\mu} \tag{5}$$

$$f = \frac{(\Delta P/L) D_h}{\frac{1}{2}\rho \bar{u}^2} \tag{6}$$

where ΔP represents the drop of pressure, $\overline{u}$ is mean flow rate at the cross-sectional area and D_h is the hydraulic diameter which can be calculated by $4A/P$, A is the cross-sectional area and P is the wetted perimeter of the cross-section.

The Newton's law of cooling can be expressed as:

$$\dot{q}_{conv} = h(T_s - T_\infty) \tag{7}$$

When the tube wall adopts the no-slip boundary condition, under the condition of constant heat flux, the heat transfer type between the wall and the near wall layer is considered to be heat conduction. The corresponding heat transfer equation can be expressed as follows:

$$\dot{q}_{conv} = \dot{q}_{input} \tag{8}$$

$$h = \frac{\dot{q}_{input}}{(T_s - T_\infty)} \tag{9}$$

$$Nu_x = \frac{h_x D_h}{k_a} \tag{10}$$

where h and k are the convective heat transfer coefficient and thermal conductivity, respectively.

$$Nu = \frac{1}{A}\int Nu_x dA \tag{11}$$

Thermal performance factor (*TPF*) represents the ratio of the heat transfer coefficient of an augmented surface (3-start spirally corrugated tube).

$$TPF = \frac{(Nu/Nu_0)}{(f/f_0)^{\frac{1}{3}}} \tag{12}$$

Nu_0 and f_0 are the Nusselt number and friction factor of the smooth straight tube, respectively.

4. Results and discussion

4.1 Smooth tube and grid validation

In order to ensure the accuracy of the calculation results, this paper compares the simulated Nusselt number and friction coefficient of the smooth tube with the theoretical values. It is well known that in laminar flow, the fluid viscosity is dominant, the flow velocity is low and the flow is stable, and the theoretical solution or empirical correlation of the Nusselt number is relatively mature. Under the constant wall temperature boundary conditions in the fully developed section, that is, the flow and temperature distribution are stable, the Nusselt number in the fully developed section of the smooth tube laminar flow is theoretically constant Nu_0 = 3.66.[27] And the product of the theoretical friction factor and the Reynolds number of the circular tube is a constant of 64.[27] The calculation formula of the friction factor and the theoretical value of the Nusselt number of the straight tube can be expressed as Eqs. (13,14):

$$f_0 = 64/Re \tag{13}$$

$$Nu_0 = 3.66 \tag{14}$$

Fig. 3 illustrates the validation of the Nusselt number and friction factor based on the results of the present calculation of the smooth tube. The values obtained by the present work and the values obtained by the exact solution are compared in the figure. It was found that the Nusselt number and friction factor have an error of less than 0.2% and 0.3%, respectively, in comparison to the exact solution. The numerical results are reliable and in good accord with the exact solution. Fig. 4 shows a fluid flow simulation in a smooth tube, conducted at five different mesh sizes (50,000, 100,000, 150,000, 200,000, and 250,000). The simulation fluid used was air, and the calculations were performed at a Reynolds number of 1,000. Table 2 shows that when the mesh size increases from 200,000 to 250,000, the Nusselt number and friction coefficient show only slight fluctuations or remain constant. The numerical

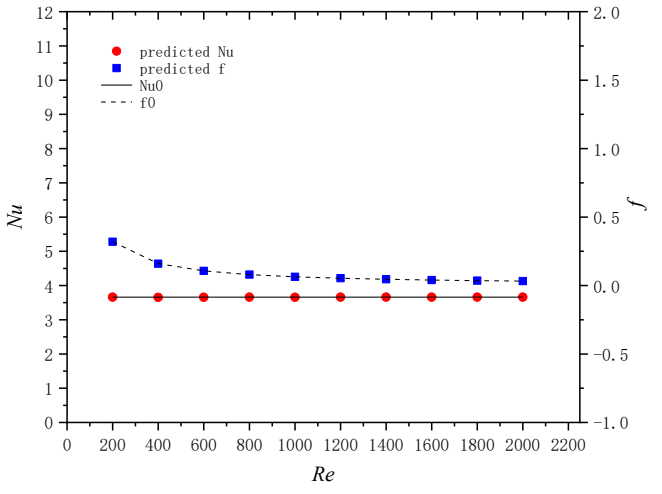

Fig. 3: Comparison of the predicted *Nu* and *f* values of present smooth tubes.

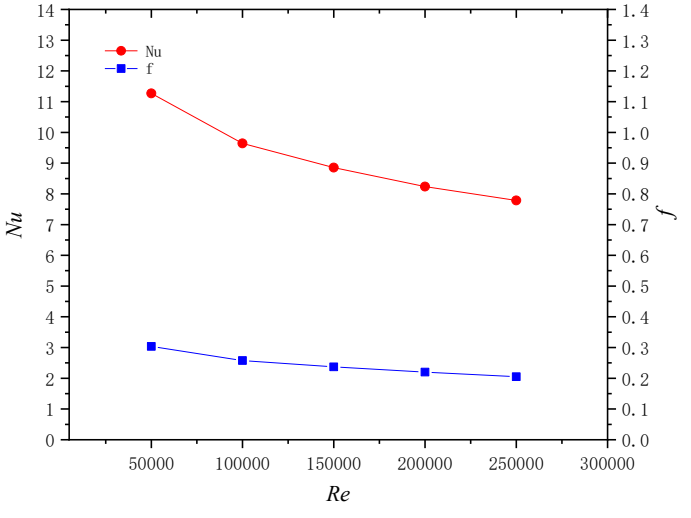

Fig. 4: Effect of grid number on fluid flow simulation of a smooth tube.

Table 2: Effect of grid independent on Nusselt number and friction factor values.

Grids numbers	*Nu*	*f*	% Error (*Nu*)	%Error (*f*)
50,000	11.2683	0.303757	14.42%	15.14%
100,000	9.642937	0.257746	8.19%	8.05%
150,000	8.853027	0.236982	6.93%	7.11%
200,000	8.238777	0.220111	5.50%	6.77%

simulation results indicate that a mesh size of 200,000 is recommended. This selection is based on the fact that mesh sizes below 200,000 can significantly deviate from the Nusselt number and friction coefficient obtained in the numerical simulation, affecting the accuracy of the results. Using a mesh size exceeding 200,000, while maintaining accuracy, consumes significant computational time and computer resources, resulting in unnecessary waste.

4.2 Heat transfer and flow in a smooth tube

Fig. 5 illustrates the flow structure and heat transfer characteristics of a smooth tube at a Reynolds number of 2000. Fig. 5(a) shows the three-dimensional flow field structure. The fluid in the tube exhibits a stable, straight-line flow pattern (streamlines parallel to the axial direction) both in the center and near the wall. This indicates a uniform velocity gradient dominated by viscous forces in laminar flow. Fig. 5(b) depicts the temperature distribution in the transverse plane of the flow and flow structure. Under constant wall temperature boundary conditions, the temperature is highest at the tube wall and gradually decreases toward the center, forming a symmetrical parabolic temperature profile. This distribution is inversely

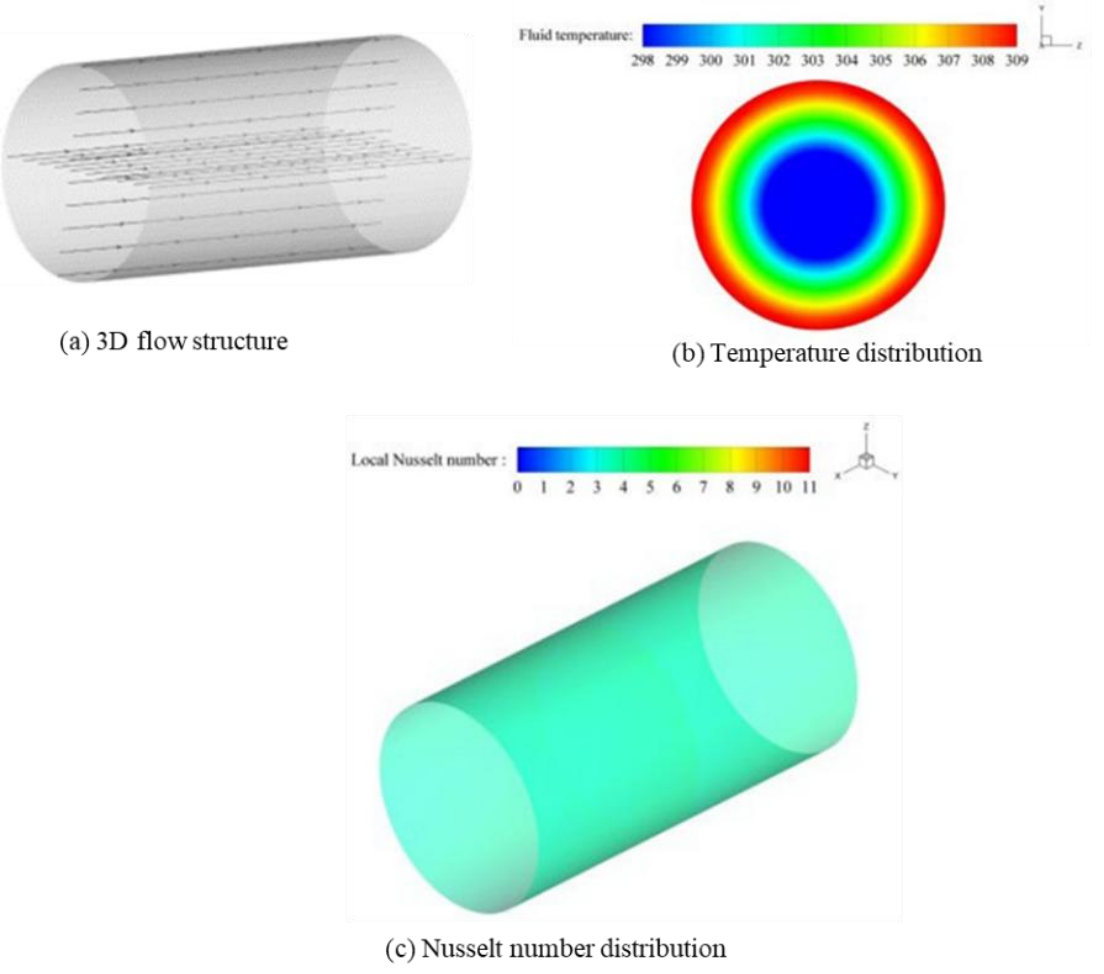

(a) 3D flow structure

(b) Temperature distribution

(c) Nusselt number distribution

Fig. 5: Flow structure and heat transfer characteristics of a smooth tube (Re = 2,000).

correlated with the velocity profile—the center has the highest velocity (strongest convective transport capacity) and the lowest temperature, while the near-wall surface, where the velocity is lowest due to viscous resistance, has the highest temperature, consistent with the principle that molecular diffusion dominates near-wall heat transfer in laminar heat transfer. Fig. 5(c) depicts the Nusselt number distribution at the tube wall. In the fully developed laminar flow section and under constant wall temperature conditions, the Nu value stabilizes near the theoretical value of 3.66 and presents a circumferentially uniform horizontal distribution curve, confirming the heat transfer uniformity brought about by the symmetry of the circular tube and indicating that the flow and thermal boundary layer have reached a stable state.

4.3 Flow and heat transfer in 3-start spirally corrugated tube

4.3.1 Effect of Reynolds number

Fig. 6 shows the three-dimensional flow structure for Reynolds numbers (Re) of 200, 1000, and 2000 when the depth ratio (DR) is 0.10 and the pitch ratio (PR) is 1.0. The 3-start spirally corrugated tube induced a continuous swirling flow along the tube. This flow pattern is characteristic of spirally corrugated walls or twisted tubes/ducts, as reported in previous studies.[17,25] A primary flow is driven by the uniform pressure gradient at the center of the tube. Near the tube wall (especially in the flutes), the tangential motion of the fluid caused by the wall constraints and the spiral structure generates a secondary flow. At a Reynolds number of 200, the flow is in a low Reynolds number regime. At this point, the fluid viscosity is significant, the swirling structure is fine and complex, the interaction between the primary and secondary flows is mild, and the turbulence intensity is low. At a Reynolds number of 1000, the inertial effect of the fluid intensifies. The swirling pattern becomes more regular, the propulsion of the primary flow is enhanced, the secondary flow develops more fully in the flutes, and the influence of turbulence on fluid mixing becomes increasingly prominent. A Reynolds number of 2000 further strengthens the dominant role of inertia. The swirl structure is clearer and more regular, the exchange of momentum between the mainstream and secondary flows is more intense, and the degree of turbulence is increased. The increased turbulence significantly enhances the mixing of fluids near the center and wall of the tube.

Fig. 7 shows the flow field temperature distribution and two-dimensional flow structure for Reynolds numbers (Re) of 200, 1000, and 2000, respectively, under the conditions of a depth ratio (DR) of 0.10 and a pitch ratio (PR) of 1.0.

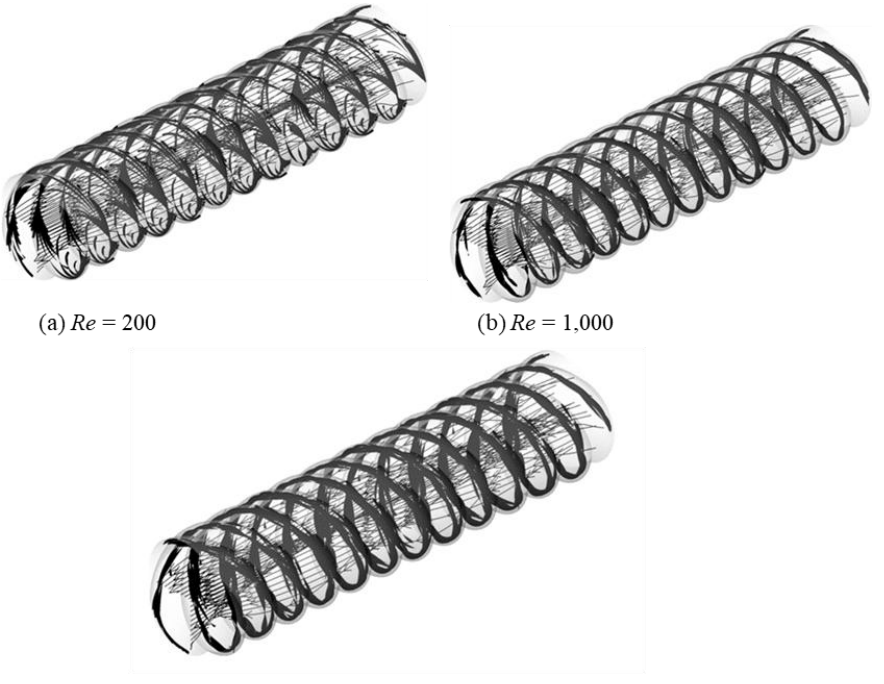

(a) Re = 200 (b) Re = 1,000

(c) Re = 2,000

Fig. 6: Influence of Reynolds number on flow structure (DR= 0.10 and PR = 1.0).

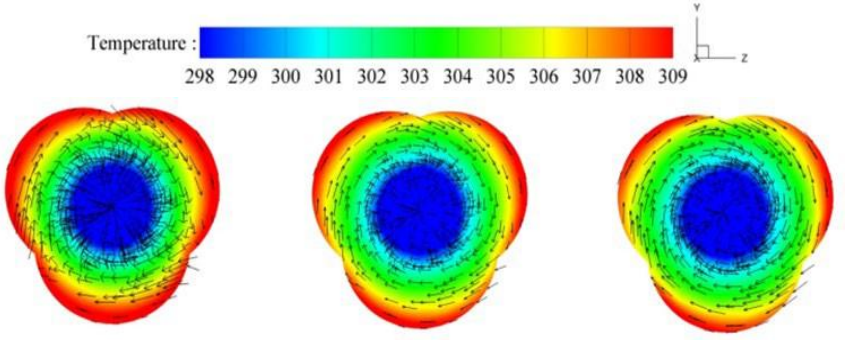

(a) Re = 200 (b) Re = 1,000 (c) Re = 2,000

Fig. 7: Influence of Reynolds number on temperature (DR= 0.10 and PR = 1.0).

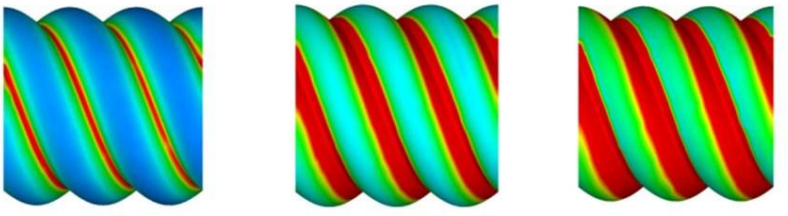

(a) Re = 200 (b) Re = 1,000 (c) Re = 2,000

Fig. 8: Influence of Reynolds number on Nusselt number distribution (DR = 0.10 and PR = 1.0).

Generally, the 3-start spirally corrugated structure generated a swirl flow on the transverse plane, which is similar pattern to that reported in.[6,17,25,26] As the Reynolds number increases, the swirl significantly thins the fluid boundary layer at the tube wall. Specifically, the cooler fluid in the center is driven by the swirl to migrate toward the tube wall. This flow behavior directly increases the fluid mixing between the fluid and the tube wall. Fig. 8 shows the distribution characteristics of the Nusselt number (Nu) at the tube wall for Reynolds numbers (Re) of 200, 1000, and 2000, respectively, under the conditions of a depth ratio (DR) of 0.10 and a pitch ratio (PR) of 1.0. The findings indicate that as the Reynolds number rises, the heat transfer at the tube wall increases accordingly. And the area of high heat transfer markedly increases with a higher Reynolds

number. The internal mechanism is that the increase in Reynolds number promotes the disturbance and flow of the fluid toward the tube wall, enhances the degree of fluid mixing, and thus makes the heat transfer process between the fluid and the tube wall more efficient.

4.3.2 Effect of pitch ratio (PR)

Fig. 9 shows the three-dimensional flow patterns for pitch ratios (PR) of 0.75, 1.0, 1.25, 1.5, 2.0, and 2.5 under the conditions of a depth ratio (DR) of 0.08 and a Reynolds number (Re) of 1600. As the PR increases, the vortex frequency decreases. This is due to a decrease in the amount of fluid entering the tube wall and a weakening of the fluid mixing, which in turn leads to a decrease in heat transfer between the low-temperature fluid in the tube core and the high-temperature fluid on the wall. Fig. 10 shows the cross-sectional two-dimensional flow pattern for the corresponding PR under the same DR and *Re* conditions. At low PR, swirl generation is more efficient at the walls and grooves, accelerating the flow swirl along the tube wall, which facilitates the destruction of the thermal boundary layer and enhances fluid mixing. Fig. 11 shows the distribution of the tube wall Nusselt number for different PRs under this condition. The smaller the PR, the more significant the heat transfer to the tube wall. This is because a larger PR reduces the fluid mixing and reduces the heat transfer between the low-temperature fluid in the tube core and the high-temperature fluid on the wall. Figs. 9-11 illustrate the influence of PR on flow and heat transfer: as the PR increases, the vortex frequency and swirl intensity will diminish, which leads to reduced fluid mixing and hindered heat exchange between the tube wall and core fluids. In contrast, a lower PR increases swirl by disrupting the thermal boundary layer, thereby enhancing heat transfer performance. These three factors together confirm the inherent coupling law between flow characteristics and heat transfer performance.

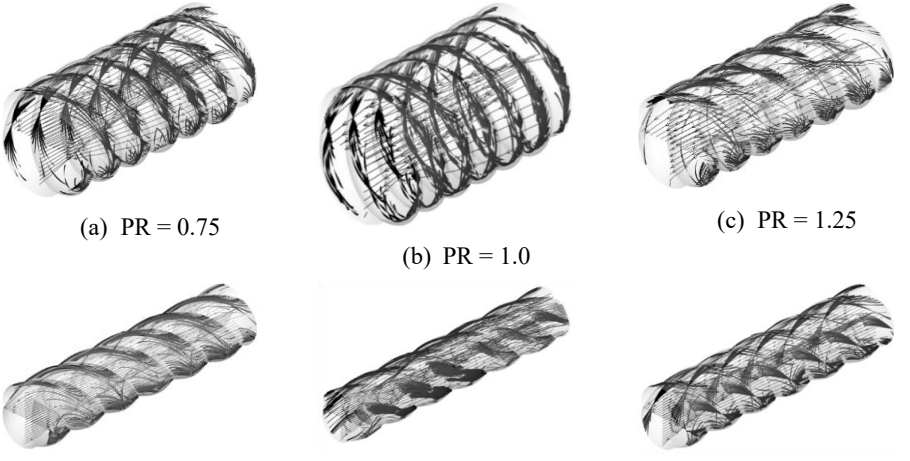

(a) PR = 0.75 (b) PR = 1.0 (c) PR = 1.25

(d) PR = 1.5 (e) PR = 2.0 (f) PR = 2.5.

Fig. 9: Influence of *PR* on three-dimensional flow pattern (*DR* = 0.08 and *Re* = 1,600).

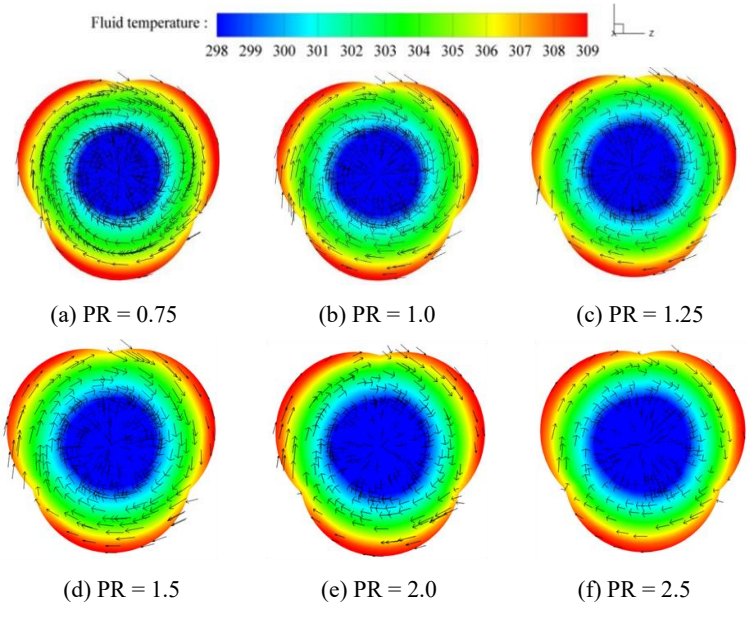

(a) PR = 0.75 (b) PR = 1.0 (c) PR = 1.25

(d) PR = 1.5 (e) PR = 2.0 (f) PR = 2.5

Fig. 10: Influence of PR on two-dimensional flow pattern (DR = 0.08 and *Re* = 1,600).

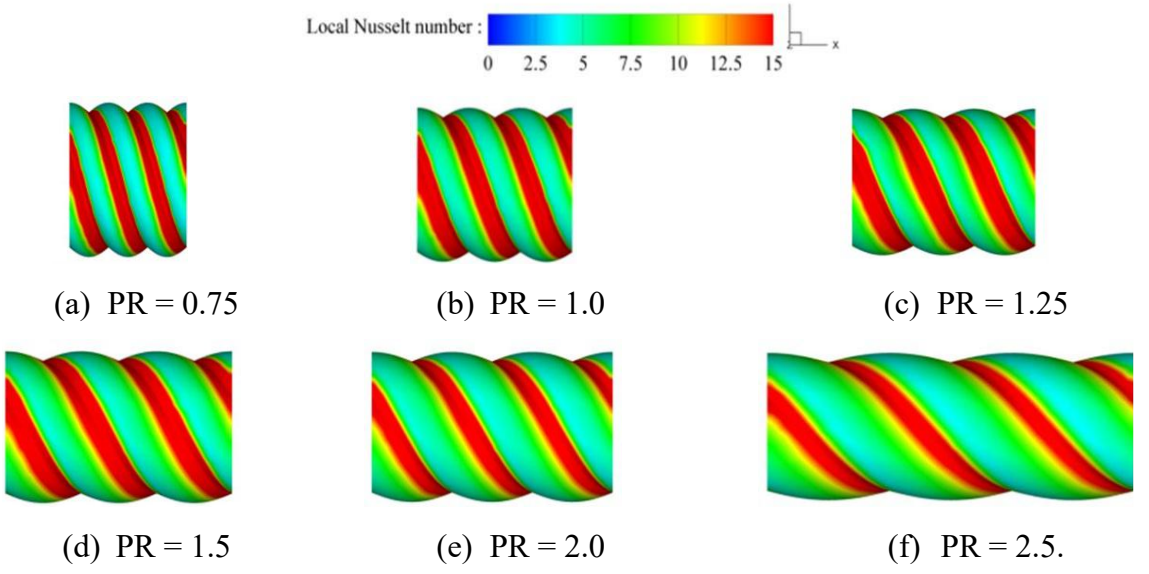

Fig. 11: Influence of PR on Nusselt number distribution (DR = 0.08 and *Re* = 1,600).

4.3.3 Effect of depth ratio (DR) on flow structures and Nusselt number distribution

Fig. 12 shows the three-dimensional flow structure for depth ratios (DR) of 0.02, 0.04, 0.06, 0.08, and 0.1 under conditions of a pitch ratio (PR) of 2.0 and a Reynolds number (*Re*) of 600. It indicates that the degree of turbulence increases with the increasing DR. Fig. 13 presents the two-dimensional cross-sectional flow pattern under the same operating conditions. As DR increases, the fluid flow undergoes more obvious deflection, separation, and reattachment. These changes promote the formation of larger vortices and secondary flows, which enhances fluid mixing and disrupts the boundary layer.

This overall process improves heat transfer efficiency. Fig. 14 shows the distribution of the Nusselt number at the tube wall under these conditions. The results show that as the DR increases, heat transfer at the tube wall also increases, as can Regions of enhanced heat transfer result from the facilitation be seen from the intensification of the red contour lines. of the flow, while regions of reduced heat transfer are associated with the flow passing through the deeper grooves. Figs. 12-14 systematically demonstrate the influence of depth ratio (DR) on flow and heat transfer, as well as the inherent correlation mechanism. The three figures mutually reinforce each other, clearly demonstrating the inherent coupling principle that DR enhances lateral mixing by increasing turbulence intensity, thereby improving heat transfer performance.

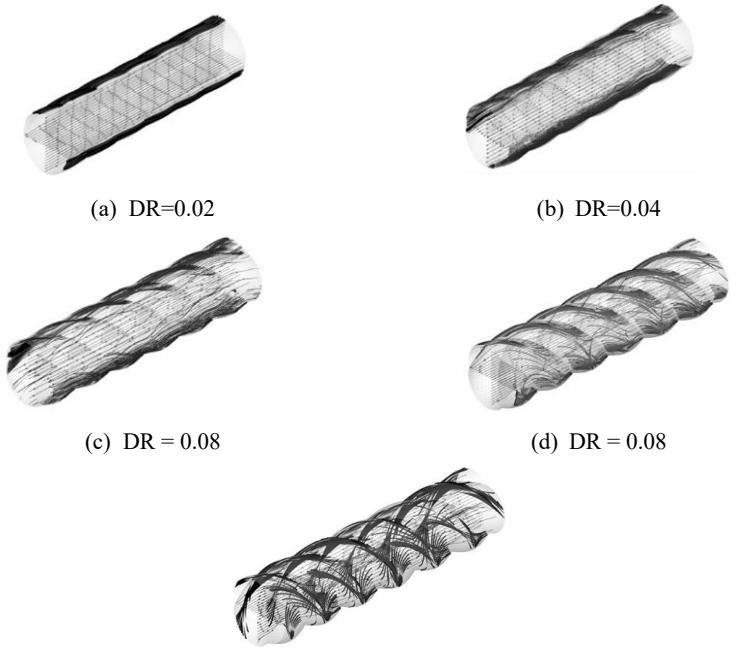

Fig. 12: Influence of DR on three-dimensional flow structure (PR = 2.0 and *Re* = 600).

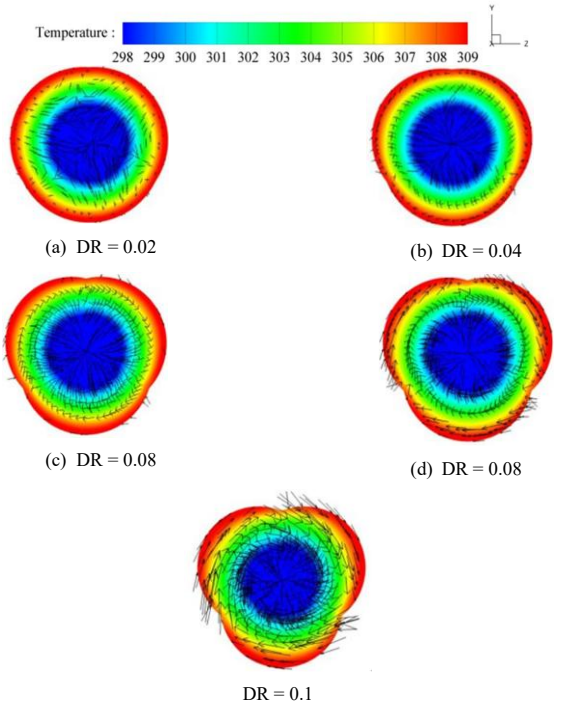

Fig. 13: Influence of DR on two-dimensional flow structure (PR = 2.0 and *Re* = 600).

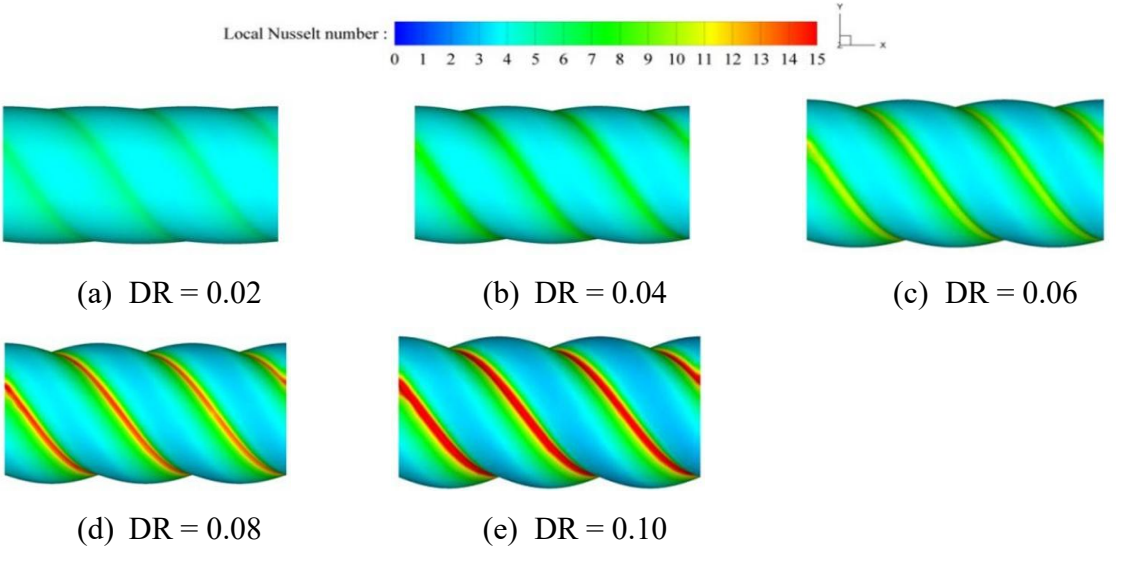

Fig. 14: Influence of DR on Nusselt number distribution (PR = 2.0 and *Re* = 600).

4.3.4 Effect of PR and DR on heat transfer

Fig. 15 shows how the Nusselt number (*Nu*) and Nusselt number ratio vary with Reynolds number (*Re*) at different pitch ratios (PR) and depth ratios. Nusselt number (*Nu*) increases with increasing Reynolds number (*Re*) at all pitch ratios (PR). For the same *Re* and PR, the greater the depth ratio (DR) of the three-lobed bellows, the higher the *Nu* value, significantly outperforming that of the smooth tube. Fig. 15(a) shows that *Nu* increases monotonically with increasing *Re* under all DR and PR conditions. This trend is consistent with the findings reported in.[6,17,25-27] Furthermore, at *Re* = 2000, under the same Re and PR conditions, Nu increases with increasing DR. Under different PR values, when *Re* = 2000 and DR = 0.1, the highest Nusselt number ranges from 11.92 to 20.25. Correspondingly, Fig. 15(b) shows that the maximum tube Nusselt number ratio, Nu/Nu_0, is achieved at Re = 2000 and DR = 0.1. As reflected in the graphs by the significant increases in *Nu* and Nu/Nu_0 with increasing DR. The phenomenon is caused by the flow characteristics such as strong vortexes and large wake vortices. Increasing DR instigates these flow characteristics. This is due to strong lateral mixing and boundary layer disruption, which greatly enhance heat transfer between the cold and hot fluids, and appeared a similar trend to that reported in.[6,17,28,29] The increase in DR provides a more sufficient momentum basis for these flow enhancement phenomena, further promoting

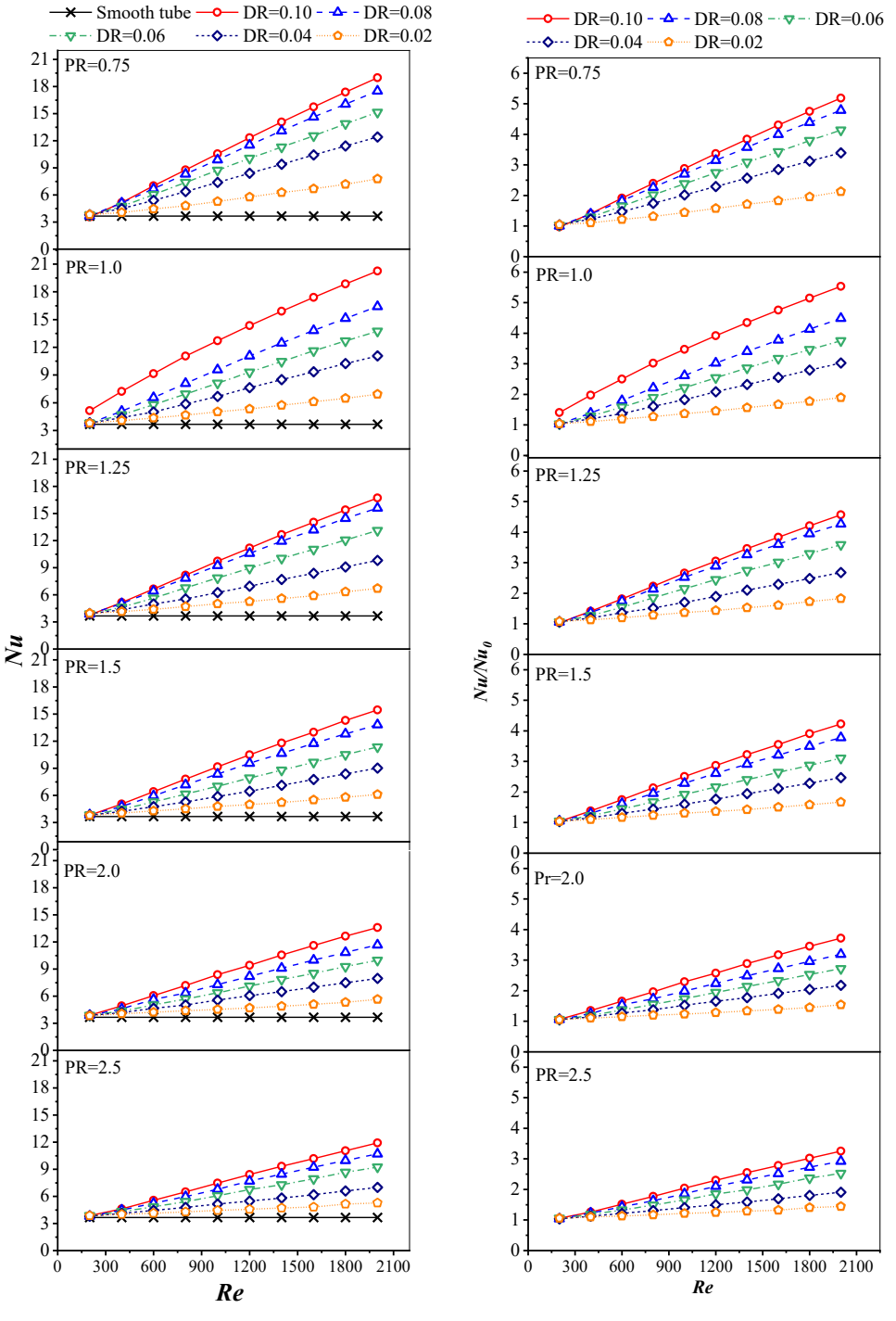

(a) *Nu* (b) *Nu/Nu₀*

Fig. 15: Effect of and DR on heat transfer.

improved heat transfer performance. When PR increases from 0.7 to 2.5, at the same *Re* and DR, the maximum *Nu* value increases from 18.98 to 20.25 and then decreases to 11.91. The maximum value of *Nu/Nu₀* rises from approximately 5.18 to 5.5 and then decreases to approximately 3.2. Under the same *Re* and DR values, a smaller PR value results in a higher heat transfer effect. This conclusion is compatible with the findings from the earlier discussion about how PR affects heat transfer and flow.

4.3.5 Effect of PR and DR on friction factor

Fig. 16 shows how the friction coefficient (*f*) and friction coefficient ratio (*f/f₀*) vary with Reynolds number (*Re*) for different pitch ratios (*PR*) and tube depth ratios (*DR*). Fig. 16(a) shows that for different pitch ratios (*PR*) and tube depth ratios (*DR*), *f* generally decreases with increasing *Re*, which similar trend to that reported in.[6,17] The larger the *DR*, the higher the value at which *f* stabilizes after decreasing. The friction factor of the smooth tubes remains low. Fig. 16(b) shows that *f/f₀*

increases with increasing *Re*, which similar trend to that reported in.[6,17] For the same *Re* and *PR*, the greater the *DR*, the higher the *f*/*f*$_0$ value. Increasing *DR* enhances fluid flow disturbance in the tube, which makes the boundary layer easy to be disrupted and increases tube wall friction. This effect is reflected in the increase in *f* and *f*/*f*$_0$ with increasing *DR*. As Re increases, the inertia of the fluid intensifies, further exacerbating this disturbance and driving a continuous increase in *f*/*f*$_0$. When PR increases from 0.75 to 2.5, at the same *Re* and *DR*, the trend of *f* is similar to that of *Nu*, fluctuating first and then decreasing. The maximum value of *f*/*f*$_0$ also shows an upward trend followed by a downward trend, and *f*/*f*$_0$ is relatively higher at smaller *PR* values. Concurrently, as *Re* and *DR* increase and *PR* decreases, the friction coefficient is higher than that of the smooth tube, with the *f*/*f*$_0$ value varying between 1.28 and 15.89 times.

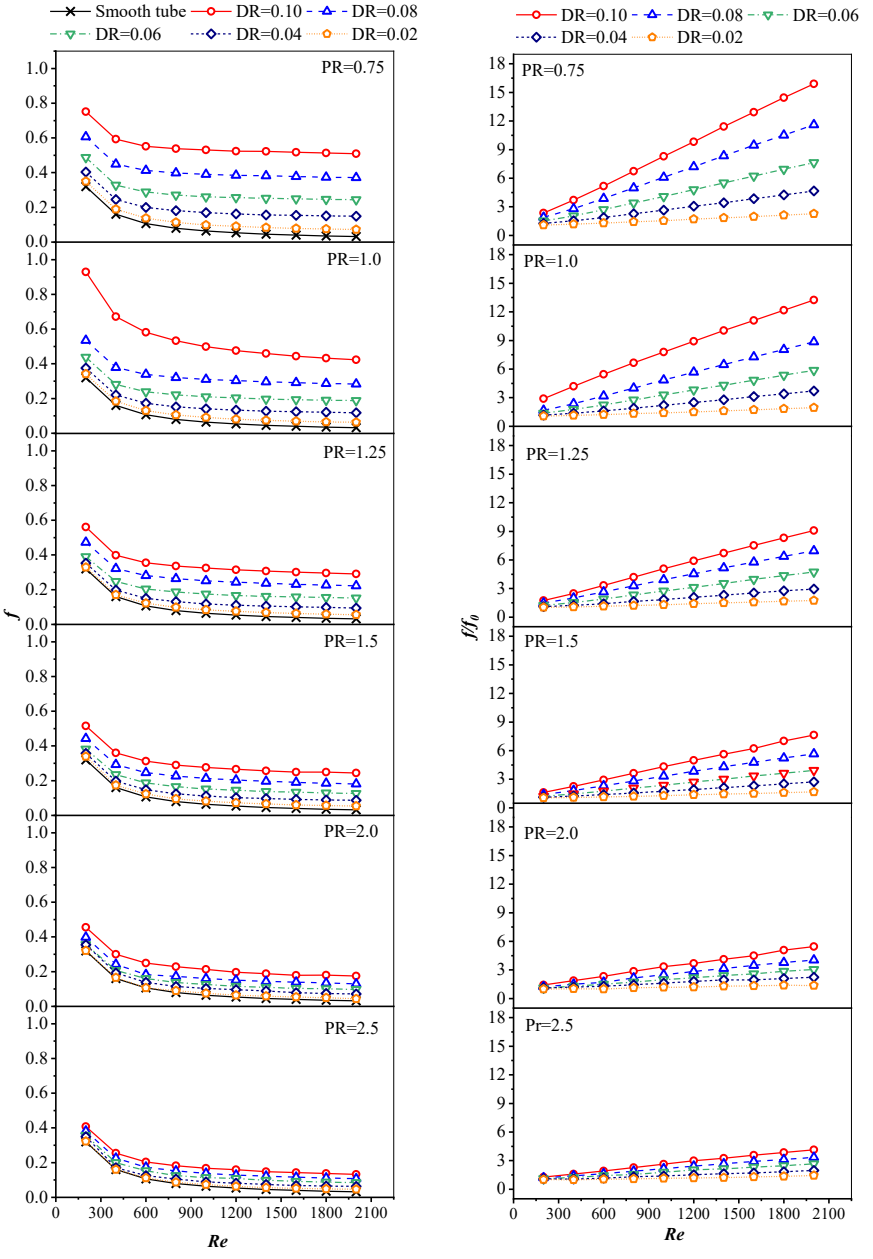

(a) *f* (b) *f*/*f*$_0$

Fig. 16: Effect of and DR on friction factor.

4.3.6 Effect of PR and DR on TPF

Fig. 17(a) shows the variation of the thermal performance factor (*TPF*) with Reynolds number (*Re*) for different pitch ratios (*PR*) and tube depth ratios (*DR*). Overall, TPF increases with increasing *Re*, which similar trend to that reported in.[6,17,25,26] This is because as Re increases, the turbulence of the fluid increases, which both enhances heat transfer (increasing *Nu*) and reduces the increase in frictional factor (*f*), resulting in a relatively gradual improvement in *TPF*. Under the same *Re* and *PR* conditions, the *TPF* increases with

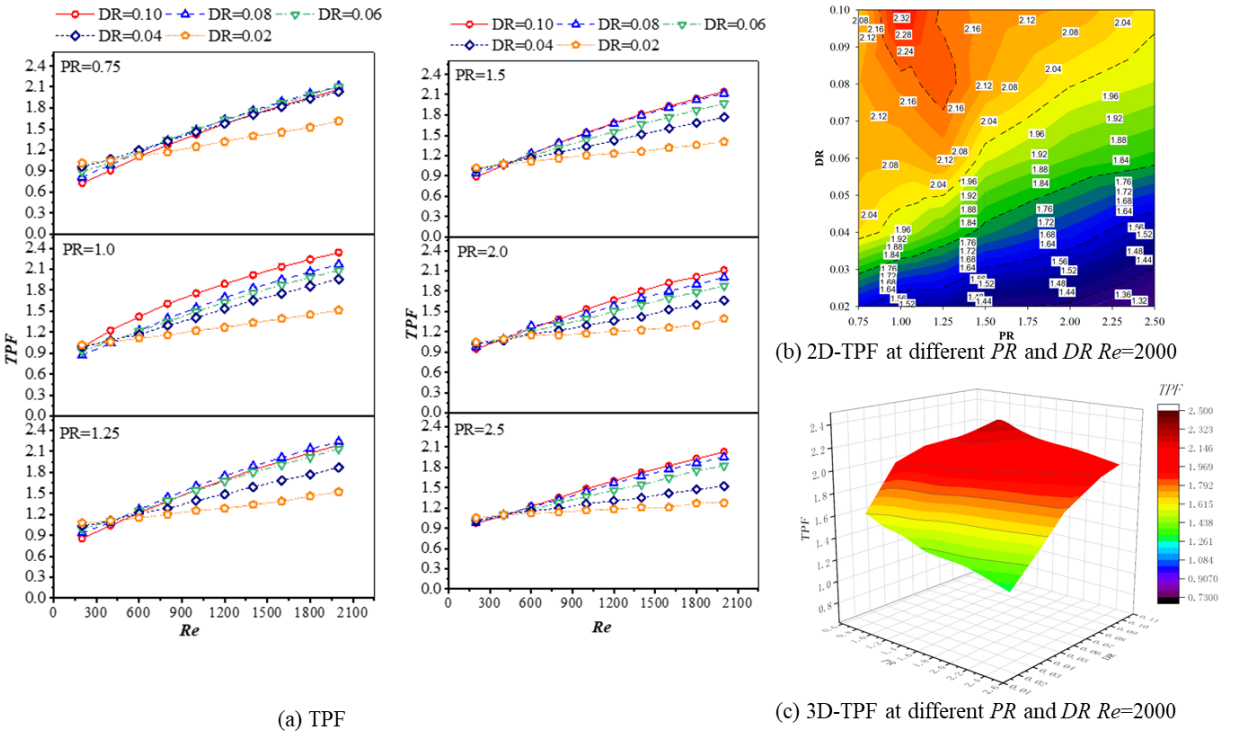

(a) TPF

(b) 2D-TPF at different *PR* and *DR* *Re*=2000

(c) 3D-TPF at different *PR* and *DR* *Re*=2000

Fig. 17: Effect of PR and DR on *TPF*.

increasing *DR*. The rising *DR* induces flow characteristics such as strong vortexes and large wake vortices within the tube. Intense lateral mixing and boundary layer disruption significantly enhance heat transfer between the hot and cold fluids. The increase in frictional factor has a relatively small negative impact on *TPF*, resulting in a significant increase in *TPF* with increasing *DR*. At the same *Re* and *DR*, the *TPF* growth trends for different *PRs* vary, but overall, the *TPF* decreases with increasing PR. At a lower Reynolds number, where, *Re* = 200, the trend of *TPR* increasing with *DR* is opposite to that at *Re* = 2000, but the overall effect on *TPF* is limited. Fig. 17(b) and 17(c) show 2D and 3D contour of *TPF* changes at *Re* = 2000, respectively, for different pitch ratios and tube depth ratios. 3D contour intuitively demonstrates the impact of different *PR* and *DR* on *TPF*. *TPF* reaches its maximum value at *PR* = 1.0 and *DR* = 0.1. This indicates that *PR* affects TPF by changing the structural characteristics of the flow in the tube. The overall thermal performance will be optimized with proper *PR* and *DR* values.

5. Comparison with previous work

The maximum TPF of the 3-start spirally corrugated tube (PR = 1.0, DR = 0.1) was compared with that reported in previous studies, including twisted square ducts combined with a twisted tape[25] and twisted elliptical tubes[8] as depicted in Fig. 18. As shown in the figure, the 3-start spirally corrugated tube achieved the highest TPF, which was approximately 28.57% and 41.57% higher than those of the twisted square ducts with a twisted tape and the twisted elliptical tubes, respectively.

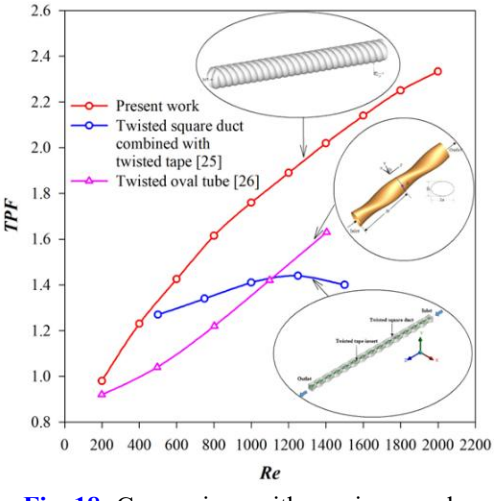

Fig. 18: Comparison with previous work.

6. Conclusion

The report presents computational results regarding the flow structure, pressure loss, and heat transfer performance factor of a 3-start corrugated tube. In the laminar flow regime, *Re* = 200 to 2,000, the effects of the pitch ratio (*PR* = 0.75, 1.0, 1.25, 1.5, 2.0, and 2.5) and five distinct depth ratios (*DR* = 0.02, 0.04, 0.06, 0.08, and 0.10) were examined. The computational results showed that the 3-start spirally corrugated tube generates helical swirl flow and main helical swirl flow, which contributes to the reduction of the thermal boundary layer thickness and the improvement of the heat transfer rate. The numerical study can be concluded as follows:

At various *DR* and *PR*, Nu rises as *Re* increases. As *Re* rises, fluid mixing and turbulence are improved, and better flow conditions for heat transfer are produced. A larger *DR* outperforms smooth tubes greatly, which yields higher *Nu* at the same *Re* and *PR*. This is due to the fact that higher *DR* causes flow features like large tail vortices and strong vortexes, which greatly improve heat transfer between the hot and cold fluids by promoting lateral mixing and severely disrupting the boundary layer. The maximum *Nu* ranges from 11.92 to 20.25 when *DR* = 0.1. As *PR* increases from 0.75 to 2.5, *Nu* initially increases and then decreases at the same *Re* and *DR*. It indicates that the smaller *PR* values will enhance heat transfer.

As *Re* increases, *f* generally decreases, while f/f_0 increases with increasing *Re*. At the same *Re* and *PR*, a larger *DR* leads to a higher value at which *f* stabilizes after decreasing, and also to a higher f/f_0 value. This fact is because an increased *DR* enhances fluid flow disturbances, increasing frictional resistance between the fluid and the tube wall. When *PR* increases from 0.75 to 2.5, at the same *Re* and *DR*, *f* first fluctuates and then decreases.

The thermal performance factor (*TPF*) increases with increasing *Re*. This is because the benefits of heat transfer enhancement outweigh the negative effects of increased frictional factor. The *TPF* value rises as *DR* increases with the same *Re* and *PR*. The effect of *PR* on *TPF* varies at the same *Re* and *DR*; the highest *TPF* of 2.33 is attained close to *PR* = 1. The results indicate that a suitable *PR* and *DR* can optimize overall thermal performance by changing the structural characteristics of the flow path within the tube. However, at low Reynolds numbers (*e.g.*, *Re* = 200), *PR* has limited effect on *TPF*.

In summary, increasing *Re* and *DR* and selecting appropriate *PR* and smaller *PR* can help improve the comprehensive thermal performance of the 3-start spirally corrugated tube and provide a theoretical basis and optimization direction for the application of bellows in the field of enhanced heat transfer.

The effects of varying the pitch ratio (*PR*) and five distinct depth ratios (*DR*) of the 3-start corrugated tube on heat transfer rate, pressure loss, and thermal performance factor characteristics were not investigated in the current research. Future research will investigate the potential of combining these 3-start corrugated tubes with twisted tape to boost the swirling flow within the core of the corrugated tube, thereby enhancing the heat transfer rate and *TPF*. We can use this information to guide the design of efficient heat exchange devices.

Acknowledgments

The research on "Characterization of heat transfer enhancement and flow topology in a three-start spirally corrugated tube" was funded by King Mongkut's Institute of Technology Ladkrabang grant number RE-KRIS/FF69/11.

Conflict of Interest

The authors declare no competing interests.

Supporting Information

Not applicable.

Nomenclature

A	Cross-sectional area, m^2 *or* heat transfer area inside tube surface a, m^3
D	Characteristic diameter of helical oval tube
DR	Depth-to-diameter ratio, (e/D)
D_h	Hydraulic diameter
f	Friction factor
h	Convective heat transfer coefficient, W m^{-2} K^{-1}
k	turbulent kinetic energy, ($k = \frac{1}{2}\overline{u_i' u_j'}$), m^2s^{-2}
k_a	thermal conductivity of air, W m^{-1} K^{-1}
Nu	Nusselt number
P	Wetted perimeter of the cross-section
PR	Pitch-to-diameter ratio, (p/D)
p	Helical oval tube pitch, m or static pressure, Pa
Pr	Prandtl number
ΔP	Drop of pressure
$\dot{q}$	Heat flux, W/m^2
Re	Reynolds number, -
T	Temperature, K
TPF	thermal performance enhancement factor, -
u_i	Velocity component in x_i-direction, m s^{-1}
u_j	Velocity component in x_i-direction, m s^{-1}
u	Velocity component in x-direction, m s^{-1}
v	Velocity component in y-direction, m s^{-1}
w	Velocity component in z-direction, m s^{-1}
$\overline{u}$	Mean flow rate at the cross-sectional area
x	Coordinate direction

Greek letters

μ	Dynamic viscosity, kg s^{-1} m^{-1}
Γ	Thermal diffusivity
ρ	density, kg m^{-3}
φ	scalar φ

Subscripts

0	smooth tube
conv	convection
i	input
s	Surface of the solid wall

∞ Fluid far from the wall

CRediT Statement

Yuexiang Du, Pitak Promthaisong and **Smith Eiamsa-ard:** Conceptualization. **Yuexiang Du** and **Pitak Promthaisong:** Methodology, Visualization. **Arnut Phila** and **Pitak Promthaisong:** Software. **Pitak Promthaisong:** Validation. **Yuexiang Du, Arnut Phila:** Formal analysis. **Yuexiang Du** and **Varesa Chuwattanakul:** Investigation, Writing. **Arnut Phila, Varesa Chuwattanakul** and **Smith Eiamsa-ard:** Resources. **Arnut Phila** and **Pitak Promthaisong:** Data curation. **Varesa Chuwattanakul** and **Smith Eiamsa-ard:** Writing - Review and editing. **Varesa Chuwattanakul** and **Smith Eiamsa-ard:** Supervision. **Yuexiang Du** and **Varesa Chuwattanakul:** Project administration. **Varesa Chuwattanakul:** Funding acquisition. All authors have read and agreed to the published version of the manuscript.

References

[1] C. Vashistha, A. K. Patil, M. Kumar, Experimental investigation of heat transfer and pressure drop in a circular tube with multiple inserts, *Applied Thermal Engineering*, 2016, **96**, 117-129, doi: 10.1016/j.applthermaleng.2015.11.077.

[2] P. Samruaisin, S. Kunlabud, K. Kunnarak, V. Chuwattanakul, S. Eiamsa-ard, Intensification of convective heat transfer and heat exchanger performance by the combined influence of a twisted tube and twisted tape, *Case Studies in Thermal Engineering*, 2019, **14**, 100489, doi: 10.1016/j.csite.2019.100489.

[3] O. Keklikcioglu, V. Ozceyhan, Experimental investigation on heat transfer enhancement of a tube with coiled-wire inserts installed with a separation from the tube wall, *International Communications in Heat and Mass Transfer*, 2016, **78**, 88-94, doi: 10.1016/j.icheatmasstransfer.2016.08.024.

[4] S. Bhattacharyya, D. K. Vishwakarma, Mixed and forced convection heat transfer and pressure drop in inclined tube with twisted tape in transition flow, *Scientific Reports*, 2025, **15**, 14018, doi: 10.1038/s41598-025-99008-6.

[5] C. Nuntadusit, M. Wae-hayee, A. Bunyajitradulya, S. Eiamsa-ard, Thermal visualization on surface with transverse perforated ribs, *International Communications in Heat and Mass Transfer*, 2012, **39**, 634-639, doi: 10.1016/j.icheatmasstransfer.2012.03.001.

[6] S. Yang, L. Zhang, H. Xu, Experimental study on convective heat transfer and flow resistance characteristics of water flow in twisted elliptical tubes, *Applied Thermal Engineering*, 2011, **31**, 2981-2991, doi: 10.1016/j.applthermaleng.2011.05.030.

[7] P. Promthaisong, W. Jedsadaratanachai, S. Eiamsa-ard, Numerical simulation and optimization of enhanced heat transfer in helical oval tubes: effect of helical oval tube modification, pitch ratio, and depth ratio, *Heat Transfer Engineering*, 2018, **39**, 1665-1685, doi: 10.1080/01457632.2017.1384281.

[8] A.-N. Guo, L.-B. Wang, Parametrization of secondary flow intensity for laminar forced convection in twisted elliptical tube and derivation of loss coefficient and Nusselt number correlations by numerical analysis, *International Journal of Thermal Sciences*, 2020, **155**, 106425, doi: 10.1016/j.ijthermalsci.2020.106425.

[9] C. Yu, H. Zhang, Y. Wang, M. Zeng, B. Gao, Numerical study on turbulent heat transfer performance of twisted oval tube with different cross sectioned wire coil, *Case Studies in Thermal Engineering*, 2020, **22**, 100759, doi: 10.1016/j.csite.2020.100759.

[10] S. Tang, L. Ding, X. Wu, J. Zhou, L. Wang, Y. Yu, Numerical investigation of thermal-hydraulic characteristics in cross-flow heat exchangers with different twisted oval tubes, *Case Studies in Thermal Engineering*, 2024, **54**, 104063, doi: 10.1016/j.csite.2024.104063.

[11] X. Li, J. Feng, Y. Tan, Z. Wang, G. Tian, L. Wang, Examination of convective heat transfer and entropy generation performance in twisted elliptical tubes using response surface method, *Applied Thermal Engineering*, 2024, **248**, 123164, doi: 10.1016/j.applthermaleng.2024.123164.

[12] A. Sheikhi Azizi, O. Jahanian, S. S. Mousavi Ajarostaghi, M. Arıcı, Employing uniform and non-uniform inner twisted elliptical tubes in a double-pipe heat exchanger, *International Journal of Heat and Fluid Flow*, 2024, **107**, 109384, doi: 10.1016/j.ijheatfluidflow.2024.109384.

[13] L. Cai, S. Mi, C. Luo, Study on enhanced heat transfer of a phase change material slurry in transverse corrugated tubes, *Applied Thermal Engineering*, 2023, **226**, 120293, doi: 10.1016/j.applthermaleng.2023.120293.

[14] F. Ahmad, S. Mahmud, M. M. Ehsan, M. Salehin, Thermo-hydrodynamic performance evaluation of double-dimpled corrugated tube using single and hybrid nanofluids, *International Journal of Thermofluids*, 2023, **17**, 100283, doi: 10.1016/j.ijft.2023.100283.

[15] J. D. Moya-Rico, A. E. Molina, J. I. Córcoles, J. A. Almendros-Ibáñez, Experimental characterization of a double tube heat exchanger with different corrugated tubes and shells, *International Journal of Thermal Sciences*, 2022, **179**, 107640, doi: 10.1016/j.ijthermalsci.2022.107640.

[16] W. Liao, S. Lian, Effect of compound corrugation on heat transfer performance of corrugated tube, *International Journal of Thermal Sciences*, 2023, **185**, 108036, doi: 10.1016/j.ijthermalsci.2022.108036.

[17] S. M. Kirkar, A. Gönül, A. Celen, A. S. Dalkilic, Multi-objective optimization of single-phase flow heat transfer characteristics in corrugated tubes, *International Journal of Thermal Sciences*, 2023, **186**, 108119, doi: 10.1016/j.ijthermalsci.2022.108119.

[18] N. Elboughdiri, S. Q. Salih, B. S. Chauhan, A. Albani, H. Almujibah, S. Islam, F. Alturise, M. A. El-Shorbagy, F. Aouaini, A. Deifalla, Numerical analysis of thermohydraulic and exergetic performance in corrugated spiral tubes with diverse arc corrugation configurations, *Case Studies in Thermal Engineering*, 2023, **51**, 103605, doi: 10.1016/j.csite.2023.103605.

[19] P. Yang, H. Zhang, Y. Zheng, Z. Fang, X. Shi, Y. Liu, Investigation and optimization of heat transfer performance of a spirally corrugated tube using the Taguchi method, *International Communications in Heat and Mass Transfer*, 2021, **127**, 105577, doi: 10.1016/j.icheatmasstransfer.2021.105577.

[20] K. Kumar, R. Kumar, R. S. Bharj, Z. Said, Effect of arc

corrugation initiation on the thermo-hydraulic performance and entropy generation of the corrugated tube, *International Communications in Heat and Mass Transfer*, 2022, **138**, 106335, doi: 10.1016/j.icheatmasstransfer.2022.106335.
[21] V. Ghazanfari, M. M. Shadman, F. Mansourzade, Y. Amini, Numerical investigation of thermal-hydraulic performance enhancement in helical coil heat exchangers with twisted tube geometries, *Case Studies in Thermal Engineering*, 2024, **60**, 104744, doi: 10.1016/j.csite.2024.104744.
[22] W. Liao, Z. Jing, S. Lian, Numerical analysis of thermal-hydraulic comprehensive performance of composite corrugated tubes with different cross-section shapes, *International Communications in Heat and Mass Transfer*, 2024, **155**, 107588, doi: 10.1016/j.icheatmasstransfer.2024.107588.
[23] M. Abdelmagied, Determining of the thermo-hydraulic characteristics and exergy analysis of a triple helical tube with inner twisted tube, *Chemical Engineering and Processing - Process Intensification*, 2024, **204**, 109922, doi: 10.1016/j.cep.2024.109922.
[24] Z. Han, H. Zhang, C. Wang, X. Zhou, Local fouling characteristics of $CaCO_3$ in corrugated tubes with different structural parameters, *International Communications in Heat and Mass Transfer*, 2024, **156**, 107651, doi: 10.1016/j.icheatmasstransfer.2024.107651.
[25] C. V P, B. Bakthavatchalam, V. Jayakumar, S. Kusekar, A. K. Pandey, K. Habib, S. Algarni, T. Alqahtani, Enhancing heat transfer in compound twisted square ducts using shortened twisted tape inserts, *Results in Engineering*, 2025, **26**, 104862, doi: 10.1016/j.rineng.2025.104862.
[26] S. V. Patankar, D. B. Spalding, A calculation procedure for heat, mass and momentum transfer in three-dimensional parabolic flows, *International Journal of Heat and Mass Transfer*, 1972, **15**, 1787-1806, doi: 10.1016/0017-9310(72)90054-3.
[27] F. Incropera and P.D. Dewitt, *Introduction to Heat Transfer*, 5th Edition, JohnWile & Sons, New York, 2006, ISBN- 978-0471457275.
[28] S. Rainieri, A. Farina, G. Pagliarini, Experimental investigation of heat transfer and pressure drop augmentation for laminar flow in spirally enhanced tubes, *2nd European Thermal-Sciences and 14th UIT Heat Transfer Conference*, Rome, 1996.
[29] A. Barba, S. Rainieri, M. Spiga, Heat transfer enhancement in a corrugated tube, *International Communications in Heat and Mass Transfer*, 2002, **29**, 313-322, doi: 10.1016/s0735-1933(02)00321-4.